Applied Catalysis B: Environmental 99 (2010) 469–477

Contents lists available at ScienceDirect

Applied Catalysis B: Environmental

journal homepage: www.elsevier.com/locate/apcatb

Fe^{+3}-doped TiO_2: A combined experimental and computational approach to the evaluation of visible light activity

Yelda Yalçın, Murat Kılıç, Zekiye Çınar*

Yıldız Technical University, Department of Chemistry, 34220 Istanbul, Turkey

ARTICLE INFO

Article history:
Available online 21 May 2010

Keywords:
TiO_2
DFT calculations
Fe^{3+}-doping
4-Nitrophenol
Heterogeneous photocatalysis

ABSTRACT

The visible light activity of TiO_2 particles was improved by Fe^{3+}-doping. In order to characterize and describe the effect of Fe^{3+}-doping on the electronic and structural properties of TiO_2, a combination of experimental structural methods and density functional theory (DFT) calculations was used. A series of Fe^{3+}-doped photocatalysts with different Fe^{3+} contents were prepared by an incipient wet impregnation method, in order to prevent penetration of the dopant cations into the bulk of TiO_2. An obvious decrease in the band-gap and a red shift of the absorption threshold were observed by UV-DRS. The Fe^{3+}-doped photocatalysts were characterized by FT-IR, XRD, Raman and XPS. The morphological structure of the photocatalysts was examined by SEM. Energy-dispersive X-ray analysis (EDX) in the SEM was also taken for the chemical analysis of the doped samples. The results indicate substitutional Fe^{3+}-doping of TiO_2. In the computational part of the study, a neutral, stoichiometric cluster $Ti_3O_8H_4$ cut from the anatase bulk structure and three new models for the substitutional Fe^{3+}-doped TiO_2 were developed. The DFT calculations were carried out by the hybrid B3LYP functional, by using double-zeta, LanL2DZ basis set. A higher photocatalytic activity for the degradation of 4-nitrophenol was obtained for the Fe^{3+}-doped TiO_2 compared to the undoped TiO_2. The results of the DFT calculations indicate that the origin of the visible light activity of the Fe^{3+}-doped TiO_2 is due to the introduction of additional electronic states within the band-gap.

1. Introduction

Global pollution problems in today's world have urged researchers to develop new techniques in the fields of environmental protection. Refractory organic compounds which are widely used in numerous processes have contaminated waste streams and surface waters. There are several conventional methods used for the removal of such pollutants, but they are not fully satisfactory for the hardly biodegradable contaminants. In the last two decades, heterogeneous photocatalysis has received much attention as a promising advanced oxidation process (AOP) for its capability to completely mineralize recalcitrant contaminants in water or air, which cannot be effectively removed by conventional methods [1–3]. This process is an efficient and economic method to decompose hazardous pollutants, because it is non-energy intensive, operates at ambient conditions and able to mineralize organic pollutants using only atmospheric oxygen as the chemical compound. Heterogeneous photocatalysis is based on the irradiation of a semiconductor with near UV-light for the generation of electron–hole (e^-/h^+) pairs that can initiate redox reactions with the adsorbed molecules on the surface of semiconductor particles, leading to complete mineralization of the pollutant molecules.

Compared to other semiconductor oxides, TiO_2 has been widely used for environmental applications, because it is chemically inert, photostable, inexpensive, non-toxic, and has high oxidative power [4,5]. However, there are still some problems in using TiO_2 as a photocatalyst such as; (i) the degradation rates for many organic pollutants have been found to be too slow to be of practical interest, because surface coverage of the photocatalyst particles is very low, (ii) TiO_2 has a wide band-gap (~3.2 eV) and thus only a small fraction of the solar spectrum (5%) is absorbed. TiO_2 is only excited by UV-light, it is inactive under visible light irradiation, (iii) due to the short charge separation distances within the particle, e^-/h^+ recombination speed is too fast resulting in a decrease in the quantum yield of the process [6]. Thus, much of the research developed in recent years has been focused on extending the optical absorption of TiO_2 to the visible region of the spectrum in order to substitute UV-light by sunlight to make use of solar energy for practical applications and enhance its photocatalytic activity by improving the separation between charge carriers.

On the other hand, the accepted mechanism of TiO_2 photocatalysis is based on the interfacial redox reactions of the photogenerated e^-/h^+ pairs on the surface of semiconductor particles. In aqueous suspension systems, electrons are trapped at

* Corresponding author. Tel.: +90 212 383 4179; fax: +90 212 383 4134.
E-mail addresses: cinarz@yildiz.edu.tr, cinarz@gmail.com (Z. Çınar).

0926-3373/$ – see front matter © 2010 Elsevier B.V. All rights reserved.
doi:10.1016/j.apcatb.2010.05.013

surface defect sites (Ti^{3+}) and removed by reactions with adsorbed molecular O_2 to produce superoxide anion radical $O_2^{\bullet-}$, while holes react with adsorbed water molecules or OH^- ions to produce OH radicals. OH radicals are considered to be the principal reactive species responsible for the photocatalytic reactions [7]. Therefore, the photocatalytic activity of TiO_2 also depends upon surface hydroxyl group density. An appropriate method to be used to enhance the photocatalytic and visible light activity of TiO_2 should be the one that can also increase the number of adsorbed surface OH groups, since OH groups are major hole scavengers.

One way to achieve these tasks is to introduce defects into TiO_2 lattice through transition metal ion doping. It has been suggested that doping with metal ions increases the photocatalytic activity of TiO_2 due to the reactions of electrons with metal ions on the surface. This reaction reduces e^-/h^+ pair recombination speed and results in an increased rate of formation of OH radicals. Among a great variety of transition metal ion dopants investigated previously [8–14], Fe^{3+} has been found to be the best candidate due to its band-gap (~2.6 eV) and similar size to that of Ti^{4+}. The ionic radii of Ti^{4+} and Fe^{3+} are 0.068 and 0.064 nm respectively [15]. Therefore, Fe^{3+} cations may insert into the TiO_2 structure and locate at interstices or occupy lattice positions. In other words, either interstitial or substitutional doping occurs. It has been believed that Fe^{3+} cations can act as shallow traps in the TiO_2 lattice and extend photo-response of TiO_2 into the visible range. However, there is a considerable controversy in the results obtained for the photocatalytic activity of Fe^{3+}-doped TiO_2. Some investigators have reported that doping with Fe^{3+} enhances the photocatalytic activity [16–19] while some research groups have found that the presence of this cation in TiO_2 is detrimental for the photocatalytic degradation reactions of organic contaminants in aqueous systems [20,21]. In some of the studies, it has been found out that the onset of absorption of the Fe^{3+}-doped photocatalyst shifts to the red region of the spectrum up to 650 nm [17]. Some researchers have claimed that Fe^{3+} doping narrows the band-gap, while others have reported that Fe^{3+} cations introduce additional electronic states into the band-gap. The amount of dopant is also controversial. Hence, the role of Fe^{3+} as a dopant in TiO_2 photocatalysis is still uncertain.

Thus, in understanding the electronic structure of Fe^{3+}-doped TiO_2, the position of the dopant and hence the effect of Fe^{3+}-doping on the band-gap, visible light and photocatalytic activity of TiO_2 it is important to use different experimental techniques together with theoretical calculations. Although different theoretical models have been developed for other transition metal ion doped TiO_2 photocatalysts, there is very limited quantum mechanical information for Fe^{3+}-doped TiO_2 in the literature [22]. In this study, we used a combination of experimental structural methods and the density functional theory (DFT) calculations to characterize and describe the effect of Fe^{3+} dopant on the electronic structure, visible light and the photocatalytic activity of TiO_2. The purpose of the computational part of the study is to provide a framework for the interpretation of the experimental data and to elucidate the structural and electronic properties of the Fe^{3+}-doped titania. The photocatalytic activity of the Fe^{3+}-doped TiO_2 was also determined by investigating the kinetics of the photocatalytic degradation of 4-nitrophenol (4-NP) in the presence of the undoped and doped TiO_2. This study may provide new insights and understanding the mechanisms of photoactivity enhancement by Fe^{3+}-doping into the lattice of TiO_2.

2. Experimental and computational details

2.1. Materials

TiO_2 Degussa P25 grade with a particle size of about 21 nm and a surface area of 50 $m^2\,g^{-1}$ was used as the photocatalyst without further treatment. Degussa P25 powder, which is a mixture of anatase and rutile phases (79% anatase, 21% rutile) is one of the photocatalysts with high activity and has been used as a standard TiO_2 reference material. The high activity is due to a synergistic effect between the two nanocrystalline phases [9]. Hombikat UV-100 (Sachtleben Chemie) was also used in order to assess the reliability of the computational results. $Fe(NO_3)_3{\cdot}9H_2O$ was purchased from Merck. All the chemicals that were used in the experiments were of laboratory reagent grade and used as received without further purification. The solutions were prepared with doubly distilled water.

2.2. Preparation of the Fe^{3+}-doped TiO_2

Doping was performed by an incipient wet impregnation method in order to prevent penetration of the dopant cations into the bulk of TiO_2, since bulk doping increases the recombination rate of charge carriers resulting in a decrease in photocatalytic activity. 8 g TiO_2 Degussa P25 and appropriate amount of $Fe(NO_3)_3{\cdot}9H_2O$ were mixed with definite volumes of doubly distilled water and stirred for 1 h. During this period, the mixture changed color into a light brownish beige depending upon the Fe^{3+} concentration. Five different Fe^{3+}-doped photocatalysts containing 0.05, 0.10, 0.25, 0.50 and 1.00 wt% Fe^{3+} were prepared. Then, the prepared photocatalysts were washed with water three times, heat-treated at

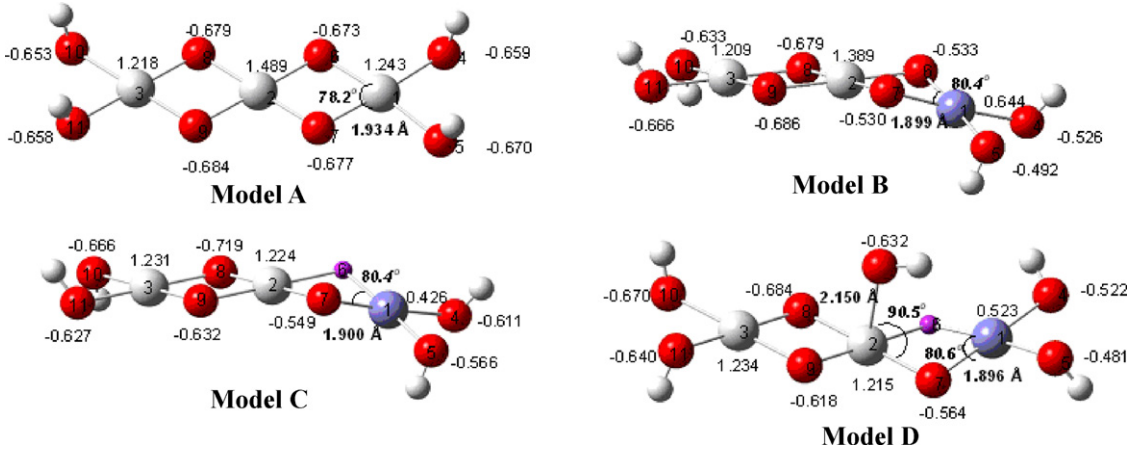

Fig. 1. Optimized structures and Mulliken charge distributions of the undoped and Fe^{3+}-doped TiO_2 clusters (grey, titanium; red, oxygen; blue, Fe^{3+}; white, hydrogen). (For interpretation of the references to color in this figure legend, the reader is referred to the web version of the article.)

373 K for 24 h to eliminate water, calcined at 773 K for 4 h, ground and sieved.

2.3. Characterization of the photocatalyst

Fourier transform infrared (FT-IR) measurements of the undoped TiO_2 and Fe^{3+}-doped TiO_2 samples were carried out in the 650–4000 cm^{-1} region with a resolution of 0.5 cm^{-1} using a Perkin Elmer Spectrum One spectrometer, the sample being in the form of KBr pellets. To examine the morphological structure of the Fe^{3+}-doped TiO_2 photocatalysts, scanning electron microscopy was performed on gold-coated samples by using a JEOL SEM apparatus. Energy-dispersive X-ray analysis (EDX) in the SEM was also taken for the chemical analysis of the doped samples. In order to determine the effect of Fe^{+3}-doping on the crystal structure of TiO_2, X-ray diffraction (XRD) patterns were obtained. XRD measurements were carried out at room temperature by using a Philips Panalytical X'Pert Pro X-ray powder diffraction spectroscope with Cu Kα radiation (λ = 1.5418 Å). The accelerating voltage and emission current were 45 kV and 40 mA respectively. The scan ranged from 20 to 70 (2θ degree) with a scan rate of 3° min^{-1}. Crystallite size was determined using the Scherrer equation:

$$L = \frac{(0.9\lambda 180)}{(\pi \mathrm{FWHM}_{hkl} \cos\ \theta)} \quad (1)$$

where $FWHM_{hkl}$ is the full width at half maximum of an *hkl* peak at θ value. The crystal structure was further analyzed by Raman spectroscopy. Raman spectra were acquired by a Perkin Elmer 400F dispersive Raman spectrometer equipped with dielectric edge filters and a cooled CCD detector. Samples were excited using a near infrared 765 nm laser pulse. The UV–visible diffuse reflectance spectra (UV-DRS) were recorded on a Perkin Elmer Lambda 35 spectrometer equipped with an integrating sphere assembly using $BaSO_4$ as the reference material. The analysis range was from 300 to 800 nm. Surface properties of the doped samples were examined by X-ray photoelectron spectroscopy (XPS). XPS measurements were performed on a SPECS ESCA system with Mg Kα source ($h\nu$ = 1253.6 eV) at 10.0 kV and 20.0 mA respectively. All the binding energies were referenced to the C 1s peak at 284.5 eV.

2.4. Photocatalytic activity experiments

The performance of the Fe^{+3}-doped TiO_2 was assessed on 4-NP by carrying out the photocatalytic degradation reactions. The photocatalytic activity experiments were carried out in a constant temperature batch-type photoreactor. 5 × 8 W blacklight fluorescent lamps were used as the light source. Total photonic fluence was determined by potassium ferrioxalate actinometer [23] as 3.1×10^{-7} Einstein s^{-1}.

In the experiments, a stock solution of 4-NP at a concentration of 1.0×10^{-2} mol L^{-1} was used. The suspension was prepared by mixing definite volumes of this solution containing the desired amount of 4-NP with TiO_2 Degussa P25 and the Fe^{+3}-doped TiO_2. The suspension was agitated in an ultrasonic bath for 15 min in the dark before introducing it into the photoreactor. The volume of the suspension was 600 mL. The amount of the photocatalyst used was 0.2 g/100 mL, which was determined as the corresponding optimum photocatalyst concentration. The suspension was stirred mechanically throughout the reaction period in order to prevent TiO_2 particles from settling. Owing to continuous cooling, the temperature of the reaction solution was 22 ± 3 °C. Under these conditions, the initial pH was at the natural pH of the compound investigated, 5.9 ± 0.2 as measured by a pH-meter (Metrohm 632). Duplicate experiments were performed unless otherwise stated.

All the samples, each 10 mL in volume were taken intermittently for analysis. The samples were then filtered through 0.45 μm cellulose acetate filters (Millipore HA). Before analyzing, all the solutions were wrapped with aluminum foil and kept in the dark. The concentration of 4-NP was measured by a UV–visible spectrophotometer (Agilent 8453) at 318 nm which was the wavelength of maximum absorption of 4-NP. The calibration curves were prepared for a concentration range $(1.0–10.0) \times 10^{-5}$ mol L^{-1} and the detection limit for 4-NP was calculated to be 3.79×10^{-6} mol L^{-1}. In the experiments, the pH of the reaction solution decreased slightly. For 120 min of degradation the change in the pH was ±0.3, which did not affect the wavelength of maximum absorption in the UV-spectrum of 4-NP.

2.5. Computational models and methodology

In order to investigate the effect of Fe^{+3}-doping on the electronic properties of TiO_2, the non-defective anatase (0 0 1) surface was modeled with a finite, neutral, stoichiometric cluster model $Ti_3O_8H_4$ (Model A), since it is the most stable surface with a high photocatalytic activity [24]. The use of neutral, stoichiometric clusters avoids the problem of associating formal charges with the cluster [25]. This cluster approach is a well-known and successful method applied in quantum mechanical calculations, because it has been determined that the size of the cluster does not have much effect on the energetics or the electronic properties of the oxide surface [26]. Fig. 1 shows the proposed models for undoped and Fe^{3+}-doped anatase clusters. The unit cell for anatase has a tetragonal structure with the bulk lattice constants $a = b = 3.78$ Å and $c = 9.51$ Å [27]. It has been experimentally determined that anatase surface is Lewis acidic due to the presence of adsorbed water molecules [6]. Water adsorption on anatase surface occurs mostly by dissociative adsorption. Therefore, in the clusters developed, the unsaturated oxygen atoms were terminated with hydrogens and titanium atoms with OH groups.

Three new models for the Fe^{3+}-doped photocatalyst $Ti_2FeO_8H_4$ were developed by quantum mechanical techniques. In Model B, the structure of the Fe^{3+}-doped TiO_2 was constructed by replacing one Ti atom whose coordination number is equal to 4 with one Fe^{3+} cation. In principle, replacing a Ti site with Fe^{3+}, an element of different charge induces a charge imbalance, thus resulting in the formation of a crystallographic point defect, an oxygen vacancy [28]. In the models developed, a dummy atom was used for the oxygen vacancy. However, the doped TiO_2 is overall electrically neutral, and the charge imbalance associated with the dopant cation can be compensated by either changing the oxidation state of an atom or by adding a group to the model. Therefore, in order to determine the best model representing the electronic structure of the Fe^{3+}-doped TiO_2 two different models were developed additionally. In Model C, a vacancy was created by the use of a dummy atom and the adjacent Ti^{4+} was converted to Ti^{3+}. Whereas, in Model D an additional OH^- ion was bound to the neighboring Ti^{4+} cation, instead of changing the oxidation state of Ti^{4+}. In the developed cluster models, all the distances are fixed at the bulk values. All the calculations were carried out using the DFT method within the GAUSSIAN 03 package [29] due to the fact that it takes electron correlation into account. The DFT calculations were performed by the hybrid B3LYP functional which combines Hartree–Fock (HF) and Becke exchange terms with the Lee–Yang–Parr correlation functional. The double-zeta LanL2DZ basis set was used in order to take the relativistic effects into account. Vibrational frequencies were calculated for the determination of all the structures as stationary points and true minima on the potential energy surfaces. All the stationary points were confirmed by the presence of positive vibrational frequencies. The cluster geometry was frozen throughout all the calculations, but the dopant, terminal hydrogens and the OH groups were relaxed. The geometric parameters, the band edges, the band-gap energies E_g and Mulliken charge distributions of the

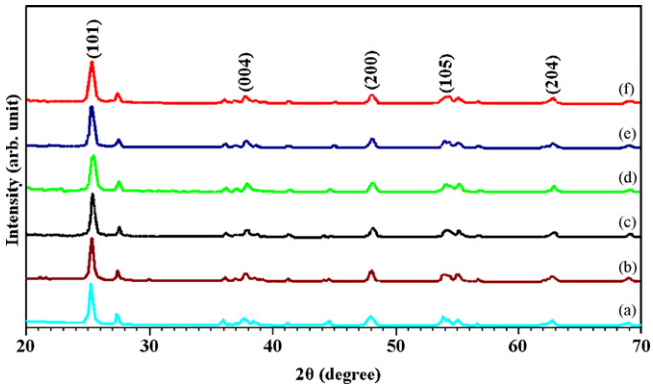

Fig. 2. XRD diffractograms of the undoped and Fe^{3+}-doped samples (a) TiO_2, (b) 0.05 wt% Fe^{3+}–TiO_2, (c) 0.1 wt% Fe^{3+}–TiO_2, (d) 0.25 wt% Fe^{3+}–TiO_2, (e) 0.5 wt% Fe^{3+}–TiO_2 and (f) 1.0 wt% Fe^{3+}–TiO_2.

atoms on the undoped and Fe^{3+}-doped photocatalyst surfaces were calculated.

3. Results and discussion

3.1. Characterization of the photocatalysts

3.1.1. X-ray diffraction

Fig. 2 shows XRD diffractograms of the undoped and Fe^{3+}-doped TiO_2 samples. The XRD diffractogram of the undoped TiO_2 (Degussa P25) shows the presence of both anatase and rutile phases. The molar fractions of both phases were calculated as 73.9% anatase and 26.1% rutile. XRD diffractogram from the Fe^{3+}-doped TiO_2 was found to be identical to that from the undoped TiO_2. This finding indicates that both rutile and anatase phases are present with the same relative amounts on the surface of the Fe^{3+}-doped sample. Any other crystalline phase containing iron could not be observed. This result reveals that due to the low calcination temperature applied in the preparation of the photocatalyst, Fe^{3+} cations do not react with TiO_2 to form new crystalline phases such as Fe_2TiO_5 and α-Fe_2O_3. The formation of these metal oxides is disadvantageous, because their photocatalytic activity is poor and they also occupy the active sites on TiO_2 surface resulting in a decrease in the number of OH radicals [30]. Compared to the undoped TiO_2, the peaks for Fe^{3+}-doped TiO_2 slightly broadened. The average crystallite sizes of the samples were estimated using the Scherrer equation and presented in Table 1. As can be seen from the values, the crystallite sizes of Fe^{3+}-doped TiO_2 are smaller than that of the undoped TiO_2, indicating a slight distortion in the crystal structure. The reason may be attributed to the formation of crystallographic point defects due to the substitution of Ti^{4+} cations by Fe^{3+} ions. The conclusion is that substitutional doping of Fe^{3+} occurs instead of interstitial doping.

Table 1
Crystallite sizes, band-gap energies E_g and absorption wavelengths λ of the undoped and Fe^{3+}-doped samples.

Samples	Particle size (nm)	Wavelength (nm)	Band-gap (eV)
Degussa P25 TiO_2	22.3	411	3.01
Hombikat UV-100	16.6	386	3.20
0.25 wt% Fe^{3+}–Hombikat	17.1	509	2.43
0.05 wt% Fe^{3+}–TiO_2	17.2	429	2.89
0.10 wt% Fe^{3+}–TiO_2	16.8	462	2.68
0.25 wt% Fe^{3+}–TiO_2	16.4	486	2.55
0.50 wt% Fe^{3+}–TiO_2	17.9	500	2.48
1.00 wt% Fe^{3+}–TiO_2	18.1	516	2.40

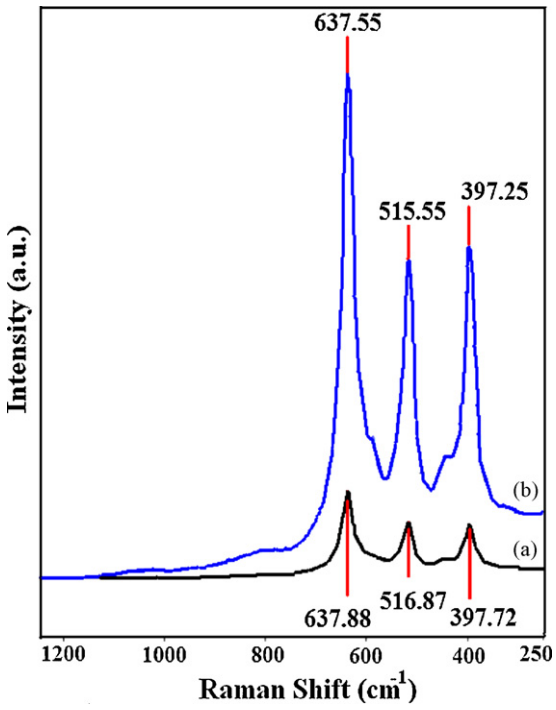

Fig. 3. Raman spectra of (a) TiO_2 and (b) 0.25 wt% Fe^{3+}–TiO_2.

3.1.2. Raman studies

Raman spectra of the undoped and Fe^{3+}-doped TiO_2 samples are shown in Fig. 3. Well-resolved Raman peaks were observed at 397 (B_{1g}), 517 (E_g) and 638 (E_g) cm^{-1} in the spectra of all the samples, indicating that anatase nanoparticles are the predominant species. No Raman lines due to iron oxide can be observed in the Fe^{3+}-doped sample, confirming the presence of the dopant cation in the substitutional positions of the crystal lattice. The results are consistent with the XRD measurements.

3.1.3. Surface morphologies

Fig. 4 shows the SEM micrographs obtained for the undoped (TiO_2 Degussa P25) and Fe^{3+}-doped TiO_2 (0.25%). As it can be seen, the undoped TiO_2 consists of homogeneous, regular and polyhedral particles. The aggregates on the surface have dimensions 5–10 μm. In contrast, the Fe^{3+}-doped TiO_2 consists of smaller particles, with straight edges and sharp corners. An examination of the surface indicates that the Fe^{3+}-doped TiO_2 is formed by particles with a very large distribution of shape and dimensions leading to a high degree of porosity. Moreover, it was observed that the size of the aggregates increases with an increase in the concentration of Fe^{3+} up to 60 μm. For the samples with high Fe^{3+} content, the aggregates were found to be homogeneous in shape and dimensions. Fig. 4(c) shows the EDX spectra of the doped samples. The obtained amount in EDX analysis was in agreement with the doping contents. No impurities were observed in the samples. The EDX results also indicate an almost uniform distribution of Fe^{3+} cations between the particles.

3.1.4. FT-IR studies

FT-IR spectra of the undoped and Fe^{3+}-doped TiO_2 are shown in Fig. 5. The spectrum for the undoped TiO_2 has a broad band in the region 3500–2400 cm^{-1} centered at around 3127.50 cm^{-1} and a strong peak at 1653.78 cm^{-1}. These peaks may be ascribed to the characteristic O–H stretching mode of OH groups and H–O–H bending mode of the adsorbed water molecules. In the region below 1071.27 cm^{-1}, there are several peaks corresponding to the

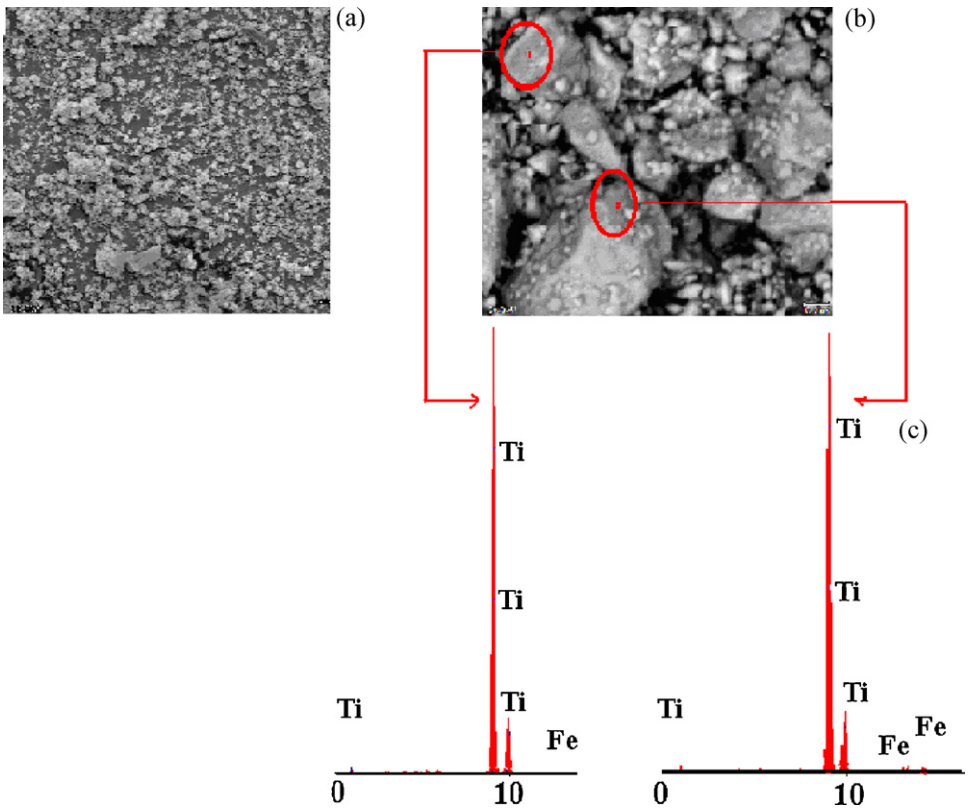

Fig. 4. SEM micrographs and EDX spectra of the undoped and Fe^{+3}-doped samples (a) TiO_2, (b) 0.25 wt% Fe^{3+}–TiO_2 and (c) EDX spectrum of 0.25 wt% Fe^{3+}–TiO_2.

absorption bands of Ti–O stretching and O–Ti–O bending vibrational modes. The Fe^{3+}-doped samples have bands associated to OH groups and TiO_2. They do not have any bands corresponding to iron phases, however a large intensity reduction was observed for the broad band at 3127.50 cm^{-1} and the one at 1653.78 cm^{-1} in the spectrum of the Fe^{3+}-doped TiO_2. This finding indicates that doped TiO_2 surface has less hydroxyl groups than the undoped TiO_2 which may be attributed to the loss of water during calcination.

3.1.5. UV–vis diffuse reflectance spectroscopy

UV–visible diffuse reflectance spectra for the undoped and Fe^{3+}-doped TiO_2 are displayed in Fig. 6. Both of the spectra have a shoulder centered at ca. 350 nm, indicating an increase in the absorption at wavelengths shorter than 400 nm. This spectral behavior can be attributed to the intrinsic absorption of TiO_2 for the excitation of valence band electrons. The spectrum for the undoped TiO_2 has a sharp absorption edge at 411 nm, however the absorption threshold of the doped TiO_2 shifted towards the visible region of the spectrum. Thus, the utility range of light is widened, which in turn may considerably increase the photocatalytic activity of TiO_2 under visible light irradiation.

Moreover, the Fe^{3+}-doped sample did not show a sharp absorption edge as observed for the undoped TiO_2. Instead, it has a long tail extending up to ca. 650 nm. The tailing of the absorption band can be assigned to the charge-transfer transition from the dopant to TiO_2 and it also explains the brownish color of the doped photocatalyst. The excitation of 3d electrons from ferric ions to the conduction band of TiO_2 is the origin of the red shift obtained in the onset of absorption of the doped photocatalyst. On the other hand,

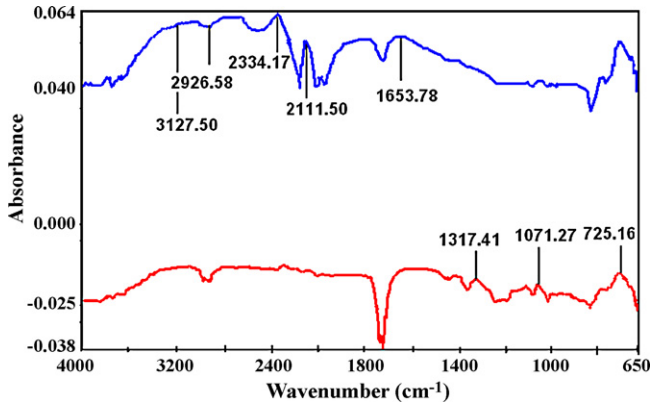

Fig. 5. FT-IR spectra of the undoped and Fe^{+3}-doped TiO_2 samples (blue, TiO_2; red, Fe^{+3}–TiO_2). (For interpretation of the references to color in this figure legend, the reader is referred to the web version of the article.)

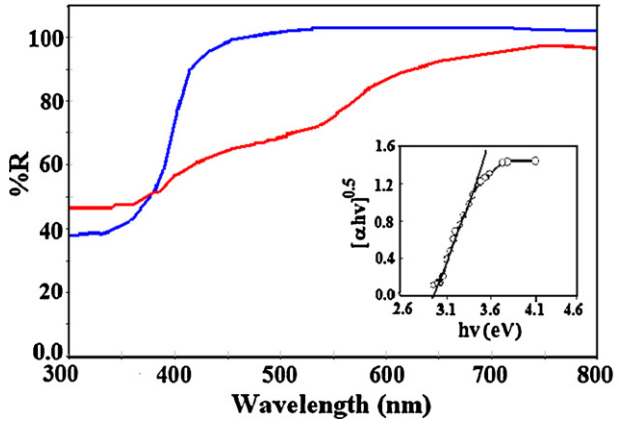

Fig. 6. UV-DRS spectra of the undoped and Fe^{+3}-doped TiO_2 samples (blue, TiO_2; red, Fe^{+3}–TiO_2). (For interpretation of the references to color in this figure legend, the reader is referred to the web version of the article.)

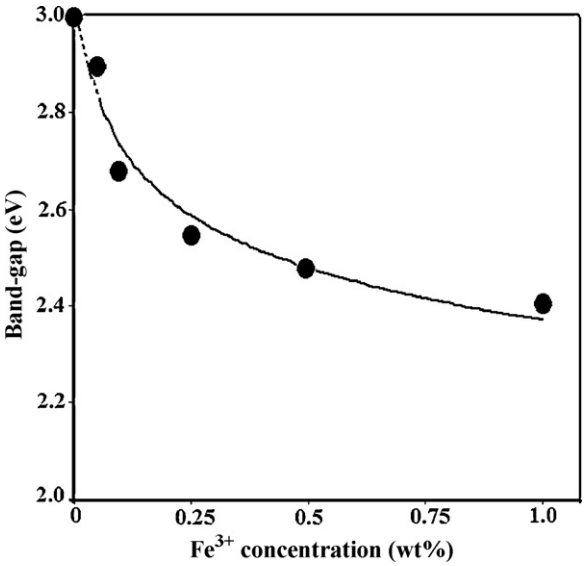

Fig. 7. Plot of the band-gap vs. Fe^{3+}-concentration of the doped samples.

the decrease of reflectance at around 550 nm may be attributed to the transition of electrons between the two levels of the five sp^3d^2 hybrid orbitals of ferric ions. In contrast to the spectrum of the undoped TiO_2, the reflectance spectrum of the doped sample has a diffused character. This would imply that Fe^{3+}-doping introduces electronic states into the band-gap of TiO_2 that are spread across the band-gap.

The band-gap energies E_g of the doped photocatalyst samples were calculated through the use of the relation between absorption coefficient α and incident photon energy $h\nu$:

$$\alpha = \frac{B_d(h\nu - E_g)^{1/2}}{h\nu} \quad (2)$$

where B_d is the absorption constant. Plots of $(\alpha h\nu)^{1/2}$ vs $h\nu$ were obtained from the spectral data of Fig. 6 and, the band-gap energies were deduced from the intersection of the linear portion extrapolation with the photon energy axis as depicted in the insert in Fig. 6. The calculated band-gap energies and the corresponding wavelengths are presented in Table 1. The values indicate that the absorbance in the visible region of the doped samples increases with the concentration of the Fe^{3+} dopant which is consistent with the changes in the color of the samples from white to brownish beige.

The relationship between the band-gap energy E_g and the Fe^{3+} content is shown in Fig. 7. It reveals that the band-gap energy decreases steeply at low Fe^{3+} concentrations. At high Fe^{3+} concentrations E_g continues decreasing but it changes much more slowly. In contrast to the results of earlier studies, an intensive study of all possible combinations of E_g and Fe^{3+} concentration (c) resulted with an exponential equation of the form:

$$E_g = 2.77e^{-0.16c} \quad (3)$$

with the correlation coefficient $r^2 = 0.97$. The relative error on E_g found by the use of Eq. (3) is only 3% on the average.

3.1.6. XPS analysis

The XPS spectra of the Fe^{3+}-doped sample (0.25% Fe^{3+}) and the undoped TiO_2 are shown in Fig. 8. The Ti $2p_{3/2}$ and Ti $2p_{1/2}$ spin-orbital splitting photoelectrons for the Fe^{3+}-doped sample are located at 461.6 and 467.6 eV respectively. No broad FWHM (full width at half maximum) of Ti $2p_{3/2}$ peak was observed. Although, there are small differences in the binding energies compared to the ones of Ti^{4+} [17], these observations indicate that titanium is in the form of Ti^{4+} in the doped photocatalyst. The small binding energy shifts to higher energies; compared to the ones in the undoped TiO_2 (460 and 465 eV) may be attributed to the formation of the Ti–O–Fe bonds in the crystal lattice. The O 1s binding energy of the doped sample is located at a higher energy than 530.5 eV corresponding to the value of the one in the undoped TiO_2, which is assigned to the metallic oxide (O^{2-}) in the TiO_2 lattice. The second small peak at 532.3 eV corresponds to the surface hydroxyl groups or chemisorbed water molecules. The signals of Fe were found to be weaker than all the others, due to the low doping level. The metallic Fe $2p_{3/2}$ peak at 707 eV was not observed. The binding energies in the range 710.4–712.3 eV were assigned to Fe $2p_{3/2}$ of Fe^{3+} cation. The results indicate that Fe^{3+} cations penetrate into the TiO_2 lattice and substitute Ti^{4+} cations; i.e. substitutional doping of Fe^{3+} occurs. The formation of the new Ti–O–Fe bonds in the crystal lattice changes the electron densities of Ti^{4+} cations and O^{2-} anions causing a change in the charge distribution of the atoms on the photocatalyst surface which may enhance the photocatalytic activity.

3.2. Photocatalytic activity

Photocatalytic activities of the Fe^{3+}-doped TiO_2 samples were evaluated by investigating the kinetics of the degradation reaction of 4-NP in aqueous suspensions. Fig. 9 shows the kinetics of disappearance of 4-NP from an initial concentration of 1.0×10^{-4} mol L^{-1} under four conditions. There was no observable loss of 4-NP when the irradiation was carried out in the absence of TiO_2 indicating that no direct photolysis takes place for 4-NP which is in agreement with our previous result [31]. In non-irradiated suspensions, there was a slight loss of 4-NP, ca. 1.0%, due to adsorption onto TiO_2 particles. However, in the presence of TiO_2, a rapid degradation of 4-NP occurred by irradiation. The concentration change amounts to 68.33% after irradiating for 120 min. We conclude that the degradation of 4-NP is due entirely to photocatalysis. The semi-logarithmic plots of concentration data gave a straight line. The correlation constant for the fitted line is $r = 0.9988$. This finding indicates that the photocatalytic degradation of 4-NP in aqueous TiO_2 suspensions can be described by the first-order kinetic model,

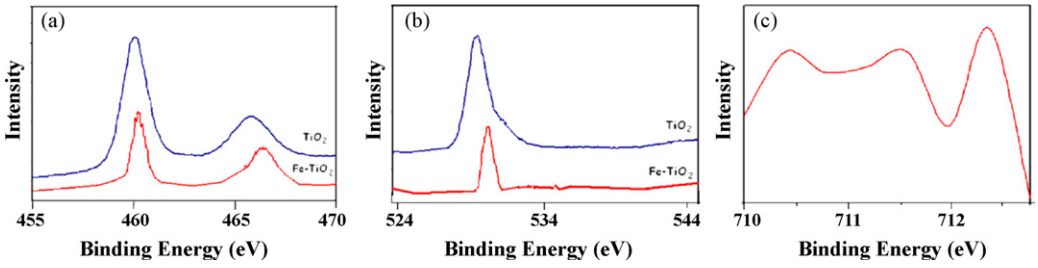

Fig. 8. XPS spectra of the undoped and Fe^{+3}-doped TiO_2 samples (a) Ti 2p, (b) O 1s and (c) Fe 2p.

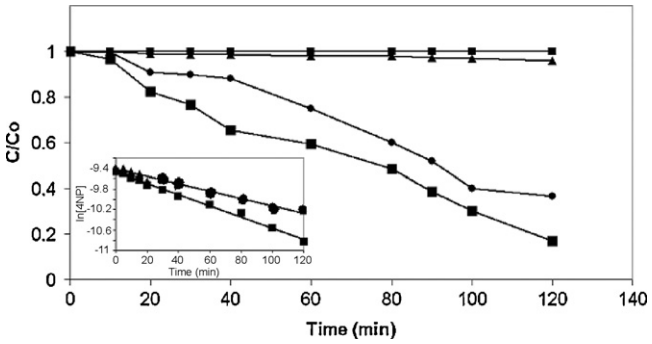

Fig. 9. Kinetics of the photocatalytic degradation of 4-NP on the undoped and. Fe^{3+}-doped TiO_2 (0.25 wt%) {(■) with light, (▲) with TiO_2, (●) with TiO_2 + light, (■) with Fe^{+3}-TiO_2}.

Table 2
Apparent first-order rate constants k for the photocatalytic degradation of 4-NP in the presence of the undoped and Fe^{3+}-doped TiO_2 samples.

% Fe	k (10^{-3} min^{-1})	r	Degradation %
0.00	12.283 ± 0.008	0.9988	68.33
0.05	14.711 ± 0.005	0.9918	63.78
0.10	19.445 ± 0.004	0.9876	69.11
0.25	28.496 ± 0.001	0.9973	80.05
0.50	22.038 ± 0.001	0.9961	72.15
1.00	18.167 ± 0.006	0.9897	70.64

$\ln C = -kt + \ln C_0$, where C_0 is the initial concentration and C is the concentration of 4-NP at time t. Under the experimental conditions used, the rate constant k for the degradation of 4-NP was calculated to be $(12.283 \pm 0.008) \times 10^{-3}$ min^{-1}.

The photocatalytic degradation reaction of 4-NP was then carried out using the Fe^{3+}-doped photocatalyst samples under the same experimental conditions. The concentration data gave a straight line, as depicted in the insert in Fig. 9, indicating that the kinetics of the degradation reaction of 4-NP in the presence of the Fe^{3+}-doped TiO_2 also obeys the first-order kinetic model. The correlation constant for the fitted line is 0.9973 for Fe^{3+}-doped TiO_2 photocatalyst. Furthermore, it also shows that the Fe^{3+}-doped TiO_2 enhances the degradation rate of 4-NP, as expected. The photocatalytic degradation rate was three times larger than that of the suspensions containing the undoped TiO_2. As a result of Fe^{3+}-doping, the rate of 4-NP degradation reaction was increased from $(12.283 \pm 0.008) \times 10^{-3}$ min^{-1} to $(28.496 \pm 0.001) \times 10^{-3}$ min^{-1}.

The results presented in Table 2 show the effect of the Fe^{3+} concentration of the doped photocatalyst on the photocatalytic degradation of 4-NP. As it can be seen from the values, the photocatalytic degradation rate of 4-NP increased and then decreased passing through the maximum degradation for the photocatalyst containing 0.25% Fe^{3+}. This result is in agreement with the suggestions reported in the literature [9,17,32]. The high photocatalytic activity of the samples with low Fe^{3+} content arises from the fact that Fe^{3+}-doping introduces vacancies in TiO_2 lattice. Oxygen vacancies on the surface favor the adsorption of water molecules and thus increase the amount of hydroxyl radicals. But, at high dopant concentrations, more electrons are transferred from the 3d orbitals of Fe^{3+} to the CB of TiO_2. Since, these electrons have lower energy than TiO_2 CB electrons; they have lower reductive power. Moreover, at high dopant concentrations, due to the decrease of the distance between trapping sites, the recombination rate of the charge carriers increases and competes with the redox reactions on the surface of the photocatalyst causing the photocatalytic activity to decrease.

Moreover, the experiments demonstrated that there is no direct correlation between the visible light activity and the photocatalytic activity. The optimum Fe^{3+} concentration was found to be 0.25%. However, the UV-DRS spectrum of this sample revealed an intermediate value of the band-gap as seen in Table 1. So, it may be concluded that visible light activity is not sufficient for a photocatalyst to be photocatalytically active. Surface reactions play a decisive role on the photocatalytic activity of the doped TiO_2s. The smallest particle size of the sample containing 0.25% Fe^{3+} among all the other Fe^{3+}-doped photocatalysts confirms this result.

3.3. Electronic structure of the Fe^{3+}-doped TiO_2 surface

The optimized structures obtained for the undoped (Model A) and Fe^{3+}-doped TiO_2 models (Model B, C and D) are presented in Fig. 1. Geometry optimizations of the models in which terminal hydrogens, OH groups and the dopant anion are relaxed gave structures with slight deviations from the original geometry of TiO_2. Comparing to the Ti–O bond in the undoped anatase, the Fe–O bond was calculated to be 0.04 Å shorter, which is consistent with the fact that the electronegativity of Fe^{3+} is higher than that of Ti^{4+}. In the three doped models developed, the shorter Fe–O bond causes the O–Fe–O angle to widen by around 2.4° as compared to the O–Ti–O angle in the undoped TiO_2. The deviations from the original geometry by around 20° show the influence of oxygen vacancies and Fe–O distortions. In Model D, the OH group was found to be oriented such that the oxygen atom locates at the top of the photocatalyst making a 90.5° angle with the surface, while the hydrogen atom points towards the lattice oxygen.

The visible light activity of a photocatalyst depends upon the magnitude of the band-gap and the presence or absence of any

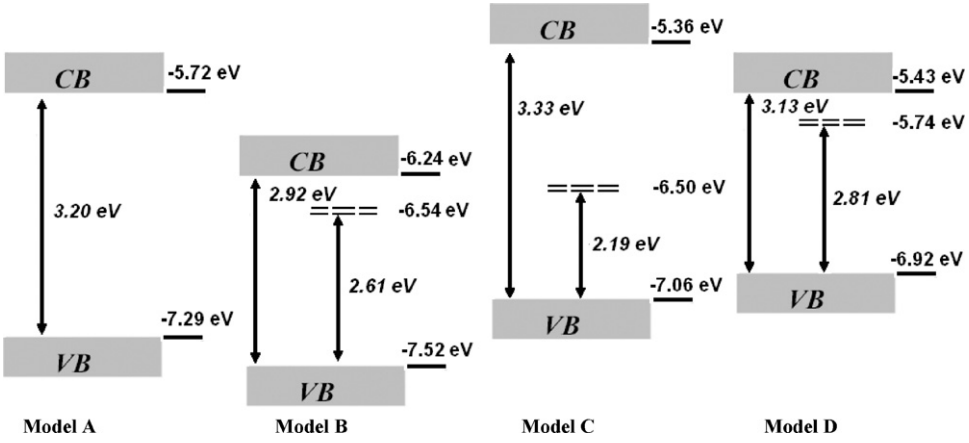

Fig. 10. Electronic structures of the undoped and Fe^{3+}-doped TiO_2 clusters computed with DFT/B3LYP method (values in italics are the corrected DFT results).

intermediate electronic states within the band-gap. The energy level diagram for the undoped and doped anatase models obtained from electronic structure calculations are displayed in Fig. 10. An examination of the values obtained for the band edges shows that the DFT/B3LYP method underestimates the band-gap energies in agreement with the earlier standard DFT results reported in the literature [25,33]. The experimental band-gap energy of the undoped TiO_2 which is around 3.2 eV was adopted as the benchmark to correct the calculated values of the anatase (0 0 1) surface. The underestimated band-gap was corrected by using a scissors operator that displaces the empty and occupied bands relative to each other by a rigid shift of 1.628 eV to bring the minimum band-gap in line with experiment. For the doped models, Models B, C and D, the corrected band-gap energies were calculated to be 2.92, 3.33 and 3.13 eV respectively. The band-gap of Model B is smaller than that of the undoped TiO_2 by about 0.28 eV, so that a red shift of the absorption threshold is possible for Fe^{3+}-doped TiO_2. In contrast, in Model C, it was observed that the formation of an oxygen vacancy causes a slight increase in the band-gap energy, by around 0.13 eV as compared to that of the undoped TiO_2. On the other hand, in Model D, the presence of an additional OH^- ion bound to the neighboring Ti^{4+} cation decreases the band-gap energy as compared to that in Model C.

The most important feature of the diagram displayed in Fig. 10 is that Fe^{3+}-doping introduces additional electronic states into the band-gap of TiO_2, in agreement with the diffused absorption spectrum of the Fe^{3+}-doped photocatalyst displayed in Fig. 6. These intermediate electronic states were determined to be mainly originating from the Fe 3d orbitals by examining the coefficients of the orbital wavefunctions. The presence of the intermediate levels separates the band-gap of TiO_2 into two parts; a wider lower gap and a significantly narrower upper gap. In Model B, the lower gap is equal to 82% of the energy gap of the undoped anatase, Model A. Although in Model C, the band-gap was calculated to be larger than that of the undoped TiO_2, the lower gap is only 69% of the band-gap energy of the undoped anatase. Therefore, it is possible to excite electrons from the VB to the intermediate energy levels by using lower energy light than that needed for the undoped TiO_2. The intermediate energy levels offer additional steps for the absorption of low energy photons through the excitation of VB electrons to these intermediate energy levels, from where they can be excited again to the CB. For the Fe^{3+}-doped TiO_2 clusters, Models B, C and D, the absorption thresholds were calculated to be 473.99, 563.86 and 440.25 nm respectively. Since the calculated value is in agreement with the experimental result obtained for Fe^{3+}-doped Hombikat UV-100 presented in Table 1, the best model representing the electronic structure of the Fe^{3+}-doped TiO_2 was determined to be Model C, indicating the formation of a vacancy along with the substitution of a Ti^{4+} cation by a Fe^{3+}. It may be concluded that the origin of the visible light activity of the Fe^{3+}-doped TiO_2 is due to the presence of additional electronic states within the band-gap. The transfer of electrons from the VB to the additional energy levels or from these levels to the CB red shifts the absorption threshold.

On the other hand, the photocatalytic activity of TiO_2 is governed by the positions of the band edges and the local charge distribution of the atoms on the photocatalyst surface. As seen from the values in Fig. 10, substitution of a Ti^{4+} cation by Fe^{3+} modifies the energies of CB and VB edges. The conduction band (CB) minimum shifts to a lower energy level in the Fe^{3+}-doped TiO_2 with respect to the undoped TiO_2 due to the electron transfer from Fe^{3+} 3d electrons to TiO_2. There is also a slight shift in the VB maximum, around 0.2 eV. Thus, the lowering of the VB edge indicates that Fe^{3+}-doped TiO_2 has a stronger oxidation power, which is consistent with the experimental result that Fe^{3+}-doped TiO_2 has a higher photocatalytic activity than does the undoped TiO_2. In Model C, the formation of a vacancy in the neighborhood of the substitutional Fe^{3+} cation has a negative effect on the band edges. The upper edge of the VB and the lower edge of the conduction band both shift to higher energies resulting in a decrease in the oxidation power of the photocatalyst. The formation of vacancies does not have any help for either the visible light activity or the oxidative power of the photocatalyst, but they enhance the photocatalytic oxidation reactions by increasing the amount of the OH radicals, as explained in Section 3.2.

Fe^{3+}-doping does not only reduce the band-gap, but it also causes a change in the local charge distribution of the atoms on TiO_2 surface. The Mulliken charge distribution of the atoms on the surface of the Fe^{3+}-doped TiO_2 models presented in Fig. 1 reveals that positive charge on Ti2 decreases. Negative charge accumulates mostly in the vacancy. The positive charge on the dopant Fe^{3+} was found to be less than that on Ti^{4+}. This finding confirms the electron transfer from Fe^{3+} to the conduction band of TiO_2. Furthermore, it also indicates that the dopant Fe^{3+} can act either as a hole or an electron trap causing the separation of the charge pairs on the surface. Thus, the dopant Fe^{3+} cation reduces the recombination rate of the charge pairs resulting in an enhancement of the photocatalytic activity of the photocatalyst.

4. Conclusions

A series of Fe^{3+}-doped TiO_2 photocatalysts have been prepared by an incipient wet impregnation method, in order to prevent penetration of the dopant cations into the bulk of TiO_2. Results of various characterization techniques indicate that Fe^{3+} cations occupy substitutional positions in the crystal lattice. The absorption threshold of the Fe^{3+}-doped photocatalyst shifts to the visible region of the spectrum. A higher photocatalytic activity for the degradation of 4-NP has been obtained for the Fe^{3+}-doped TiO_2 compared to the undoped TiO_2. The experiments have demonstrated that there is no direct correlation between the visible light activity and the photocatalytic activity. The sample with 0.25% Fe^{3+} content has been determined to have the highest photocatalytic activity mainly due to its smallest particle size among the samples prepared. The high photocatalytic activity of the samples with low Fe^{3+} content arises from the fact that Fe^{3+}-doping introduces vacancies in TiO_2 lattice and lowers the VB maximum as well. Eventually, on the basis of experimental results combined with DFT calculations, it may be concluded that the origin of the visible light activity of the Fe^{3+}-doped TiO_2 is due to the introduction of additional electronic states within the band-gap.

Acknowledgements

The authors express their thanks to Yıldız Technical University Research Foundation for financial support (Project No: 24-01-02-11) and to Degussa Limited Company in Turkey for the generous gift of TiO_2 Degussa P25.

References

[1] A. Mills, S. Le Hunte, J. Photochem. Photobiol. A 108 (1997) 1–35.
[2] D. Bahnemann, J. Cunningham, M.A. Fox, E. Pelizzetti, P Pichat, N. Serpone, in: G.R. Helz, R.G. Zepp, D.G. Crosby (Eds.), Aquatic and Surface Photochemistry, Lewis, Baco Raton, FL, 1994, p. 261.
[3] P Pichat, in: G. Ertl, H. Knözinger, J. Weitkamp (Eds.), Handbook of Heterogeneous Photo-Catalysis, vol. 4, VCH, Weinheim, 1997, p. 2111.
[4] D.F. Ollis, E. Pelizzetti, N. Serpone, Environ. Sci. Technol. 25 (1991) 1523–1529.
[5] D.W. Bahnemann, D. Bockelmann, R. Goslich, Sol. Energy Mater. 24 (1991) 564–583.
[6] M. Kılıç, Z. Çınar, J. Adv. Oxid. Technol. 12 (1) (2009) 37–46.
[7] T. Xu, P.V. Kamat, S. Joshi, A.M. Mebel, Y. Cai, K.E. O'Shea, J. Phys. Chem. A 111 (2007) 7819–7824.
[8] K. Nagaveni, M.S. Hegde, G. Madras, J. Phys. Chem. B 108 (2004) 20204–20212.
[9] P. Bouras, E. Stathatos, P. Lianos, Appl. Catal. B: Environ. 73 (2007) 51–59.
[10] Y. Wu, J. Zhang, L. Xiao, F. Chen, Appl. Catal. B: Environ. 88 (3) (2009) 525–532.
[11] K. Melghit, O.S. Al-Shukeili, I. Al-Amri, Ceram. Int. 35 (2009) 433–439.

[12] G. Bin-Daar, M.P. Dare-Edwards, J.B. Goodenough, A. Hamnett, J. Chem. Soc., Faraday Trans. 1 (79) (1983) 1199–1213.
[13] J.G. Highfield, P. Pichat, New J. Chem. 13 (1989) 61–66.
[14] A. Fuerte, M.D. Hernández-Alonso, A.J. Maria, A. Martínez-Arias, M. Fernández-García, J.C. Conesa, J. Soria, Chem. Commun. (2001) 2718–2719.
[15] M.C. Wang, H.J. Lin, T.S. Yang, J. Alloys Compd. 473 (2009) 394–400.
[16] C. Wang, C. Böttcher, D.W. Bahnemann, J.K. Dohrmann, J. Mater. Chem. 13 (2003) 2322–2329.
[17] J. Zhu, F. Chen, J. Zhang, H. Chen, M. Anpo, J. Photochem. Photobiol. A. Chem. 180 (2006) 196–204.
[18] W.C. Hung, Y.C. Chen, H. Chu, T.K. Tseng, Appl. Surf. Sci. 255 (2008) 2205–2213.
[19] M.A. Khan, S.I. Woo, O.B. Yang, Int. J. Hydrogen Energy 33 (2008) 5345–5351.
[20] C. Adan, A. Bahamonde, M.F. Garcia, A.M. Arias, Appl. Catal. B: Environ. 72 (2007) 11–17.
[21] Z. Li, W. Shen, W. He, X. Zu, J. Hazard. Mater. 155 (2008) 590–594.
[22] G. Shao, J. Phys. Chem. C 112 (2008) 18677–18685.
[23] J.G. Calvert, J.N. Pitts, Photochemistry, Wiley, New York, 1966, pp. 783–786.
[24] T. Homann, T. Bredow, K. Jug, Surf. Sci. 555 (2004) 135–144.
[25] T. Bredow, G. Pacchioni, Surf. Sci. 426 (1999) 106–122.
[26] I. Onal, S. Soyer, S. Senkan, Surf. Sci. 600 (2006) 2457–2469.
[27] T. Sekiya, M. Igarashi, S. Kurita, S. Tokekawa, M. Fujisawa, J. Electron. Spectrosc. Relat. Phenom 92 (1–3) (1998) 247–250.
[28] K. Yang, Y. Dai, B. Huang, M.H. Whangbo, Chem. Mater. 20 (2008) 6528–6534.
[29] M.J. Frisch, G.W. Trucks, H.B. Schlegel, G.E. Scuseria, M.A. Robb, J.R. Cheeseman, J.A. Montgomery, Jr., T. Vreven, K.N. Kudin, J.C. Burant, J.M. Millam, S.S. Iyengar, J. Tomasi, V. Barone, B. Mennucci, M. Cossi, G. Scalmani, N. Rega, G.A. Petersson, H. Nakatsuji, M. Hada, M. Ehara, K. Toyota, R. Fukuda, J. Hasegawa, M. Ishida, T. Nakajima, Y. Honda, O. Kitao, H. Nakai, M. Klene, X. Li, J.E. Knox, H.P. Hratchian, J.B. Cross, C. Adamo, J. Jaramillo, R. Gomperts, R.E. Stratmann, O. Yazyev, A.J. Austin, R. Cammi, C. Pomelli, J.W. Ochterski, P.Y. Ayala, K. Morokuma, G.A. Voth, P. Salvador, J.J. Dannenberg, V.G. Zakrzewski, S. Dapprich, A.D. Daniels, M.C. Strain, O. Farkas, D.K. Malick, A.D. Rabuck, K. Raghavachari, J.B. Foresman, J.V. Ortiz, Q. Cui, A.G. Baboul, S. Clifford, J. Cioslowski, B.B. Stefanov, G. Liu, A. Liashenko, P. Piskorz, I. Komaromi, R.L. Martin, D.J. Fox, T. Keith, M.A. Al-Laham, C.Y. Peng, A. Nanayakkara, M. Challacombe, P.M.W. Gill, B. Johnson, W. Chen, M.W. Wong, C. Gonzalez, J.A. Pople, Gaussian 03, B01 Gaussian, Inc., Pittsburgh PA, 2003.
[30] J.A. Wang, R.L. Ballesteros, T. Lopez, A. Moreno, R. Gomez, O. Novaro, X. Bokhimi, J. Phys. Chem. 105 (2001) 9692–9698.
[31] N. San, A. Hatipoglu, G. Koçtürk, Z. Çınar, J. Photochem. Photobiol. A:Chem. 146 (3) (2002) 189–197.
[32] Z. Zhang, C.C. Wang, R. Zakaria, J.Y. Ying, J. Phys. Chem. B 102 (1998) 10871–10878.
[33] J. Di Valentin, E. Finazzi, G. Pacchioni, A. Selloni, S. Livraghi, M.C. Paganini, E. Giamello, Chem. Phys. 339 (2007) 44–56.